JOURNAL OF SOLID STATE CHEMISTRY **140,** 182–193 (1998)
ARTICLE NO. SC987848

High-Pressure Synthesis, Crystal Structure, and Metal–Semiconductor Transitions in the $Tl_2Ru_2O_{7-\delta}$ Pyrochlore

T. Takeda, M. Nagata, H. Kobayashi, R. Kanno,[1] and Y. Kawamoto

Department of Chemistry, Faculty of Science, Kobe University, Nada, Kobe, Hyogo 657, Japan

M. Takano

Institute for Chemical Research, Kyoto University, Uji, Kyoto 611, Japan

T. Kamiyama

Institute of Materials Science, University of Tsukuba, Tennodai, Tsukuba, Ibaraki 305, Japan

F. Izumi

National Institute for Research in Inorganic Materials, 1-1 Namiki, Tsukuba, Ibaraki 305, Japan

and

A. W. Sleight

Department of Chemistry, Oregon State University, Corvallis, Oregon 97330

Received November 12, 1997; in revised form April 1, 1998; accepted April 15, 1998

Thallium ruthenium oxides, $Tl_2Ru_2O_{7-\delta}$, with the pyrochlore structure were synthesized under a pressure of 1–5 GPa and 1173 K and characterized by resistivity, magnetization, and TOF neutron-diffraction measurements. The oxygen vacancy, δ, varied with the synthesis conditions and significantly affected their electrical properties. The pyrochlores synthesized at high pressure and atmospheric pressure are classified into four groups which depend on their oxygen nonstoichiometry. (i) Nonstoichiometric $Tl_2Ru_2O_{6.71}$ shows a metallic conductivity with almost temperature-independent magnetization. (ii) Stoichiometric $Tl_2Ru_2O_7$ synthesized under high oxygen pressure using $KClO_4$ shows a metallic–semiconducting transition at 120 K with magnetization anomalies at 120 and 40 K. (iii) Slightly nonstoichiometric $Tl_2Ru_2O_{6.96}$ shows spin-glass-like behavior around 40 K accompanying a resistivity increase at the transition. (iv) $Tl_2Ru_2O_7$ synthesized at 773 K and atmospheric pressure is semiconducting with magnetization anomalies at 120 and 40 K. The change from the metallic to semiconducting state is discussed from the viewpoint of structure changes. © 1998 Academic Press

1. INTRODUCTION

The pyrochlores $A_2Ru_2O_7$ exhibit a wide range of electrical resistivities: $Bi_2Ru_2O_7$ and $Pb_2Ru_2O_{6.5}$ are metallic and Pauli paramagnetic with low resistivities of $10^{-3}\ \Omega\cdot$cm at room temperature; $Ln_2Ru_2O_7$ (Ln = Pr–Lu) and $Y_2Ru_2O_7$ are semiconducting with low activation energies (1–3); and $Tl_2Ru_2O_{7-\delta}$ shows a metallic–semiconducting transition around 120 K (4, 5). To understand their high electrical conductivities, the electronic structures of $Bi_2Ru_2O_7$, $Y_2Ru_2O_7$, and $Pb_2Ru_2O_{6.5}$ have been investigated by XPS, UPS, and HREELS (6–8) and by the pseudofunction method (9). The unoccupied Pb or Bi 6*p* states are close to E_F and contribute to the metallic conductivity by mixing with the Ru 4*d* state via the framework oxygen. On the other hand, relationships between the electrical properties and the crystal structures have been reported for the solid solutions, $Bi_{2-x}Ln_xRu_2O_7$ and $Pb_{2-x}Ln_xRu_2O_{7-\delta}$ (Ln = Y, Pr–Lu) (10–12). The metallic–semiconducting change is related to their structural changes as follows: the Ru–O(1) bond length in the RuO_6 octahedra increases, (ii) the distortion of the RuO_6 octahedra increases, and (iii) the bend in the RuO_6 zigzag chains increases with increasing Ln^{3+} contents.

The thallium pyrochlore was first synthesized by Sleight *et al.* (4) under 0.3 GPa of applied pressure. $Tl_2Ru_2O_7$

[1]To whom correspondence should be addressed.

0022-4596/98 $25.00

showed metallic properties with nearly temperature independent resistivity. Later, Jarrett *et al.* (5) reported that $Tl_2Ru_2O_{7-\delta}$ synthesized at high pressure showed a metallic–semiconducting transition around 120 K. However, the transition behavior in the system was quite complicated. The transition temperature varied with their lattice parameters. They suggested that three regions appear as the lattice parameter a decreases: (i) a metallic region, (ii) an enhanced susceptibility region, and (iii) a metallic–semiconducting transition region. However, the relationships between the structures, the compositions, and their physical properties are still ambiguous.

The thallium pyrochlore tends to be off stoichiometry. The composition, δ, in $Tl_2Ru_2O_{7-\delta}$ is difficult to determine chemically because the sample is insoluble in any acids. Furthermore, systematic control of oxygen stoichiometry in syntheses is difficult because of the high vapor pressure of thallium oxide; the reaction at atmospheric pressure is controlled by gaseous species of the thallium oxide, Tl_2O, and the following redox–vaporization process is active above 873 K: $Tl_2O_3 \rightleftharpoons Tl_2O + O_2$.

Previously, we synthesized the thallium pyrochlore at atmospheric pressure and found a low-temperature phase, $Tl_2Ru_2O_7$ (synthesized at 773 K), and a high-temperature phase, $Tl_2Ru_2O_{6.71}$ (synthesized at 1173 K), which are semiconducting and metallic, respectively (13). However, no metallic–semiconducting transition was observed around 120 K; the low-temperature phase with nearly stoichiometric composition might be different from those reported by Jarrett *et al.* (5). Synthesis above 1173 K at atmospheric pressure is difficult because of a complete decomposition from $Tl_2Ru_2O_{7-\delta}$ to RuO_2 and Tl_2O. A high-pressure technique is necessary to control the reaction.

In the present study, the thallium pyrochlores were synthesized under high-pressure and high-oxygen-pressure conditions (1–5 GPa). The synthesis conditions were changed systematically and the relationships between the conditions, compositions of the reaction products, their physical properties, and the structures were clarified. Furthermore, phase transitions in $Tl_2Ru_2O_7$ and $Tl_2Ru_2O_{6.96}$ were studied with low-temperature X-ray diffraction measurements.

2. EXPERIMENTAL

Starting materials were RuO_2, Tl_2O_3, and Ru (RuO_2, Ru, Furuuchi Chemical Ind. Ltd., $> 99.99\%$ purity; Tl_2O_3, Nakarai Chemicals Ltd., $> 99.9\%$ purity). These were weighed, mixed, and put into a sandwich-type gold capsule. The cell was then inserted in a piston–cylinder type high-pressure apparatus and heated for 1 h at a fixed temperature of 1173–1373 K and a pressure of 1–5 GPa. In order to apply high oxygen pressure, the sample was put into a gold capsule with an oxidizing agent, $KClO_4$, either mixed with each other or separated with a stabilized ZrO_2 powder which prevented reaction between the oxides on both sides.

X-ray diffraction patterns of the powdered samples were obtained with an X-ray diffractometer (Rigaku RAD-C, 12 kW) with Cu$K\alpha$ radiation. The lattice parameters of the thallium pyrochlores were refined by Rietveld analysis using the computer program RIETAN-94 (14). The diffraction data were collected for 5 s at each 0.02° step width over a 2θ range from 10 to 100°. X-ray diffraction data were taken at 10–300 K.

Neutron-diffraction data were taken at 295 K on a time-of-flight (TOF) neutron powder diffractometer, VEGA, at the KENS pulsed spallation neutron source at the National Laboratory for High Energy Physics (KEK) (15). The specimen (ca. 1 g) was contained in a cylindrical vanadium cell of dimensions 5 mm in radius, 55 mm in height, and 200 μm in thickness. The structural parameters were refined with RIETAN-96T.

Electrical resistivity was measured for the samples with dimensions of approximately $2 \times 2 \times 3$ mm. The data were obtained by the dc four-probe method with silver-paste contact in the temperature range $10 \leq T \leq 300$ K using a Toyo-Sanso low-temperature electrical-conductivity measurement unit. Magnetization was measured by a SQUID magnetometer (Quantum Design, MPMS2) at between 5 and 300 K in a field of 1 kOe.

3. RESULTS AND DISCUSSION

3.1. Synthesis

Thallium pyrochlores were synthesized with various starting compositions and reaction conditions. Reactions under high pressure in a closed vessel might control the amount of vacancies in the reaction products. Compositions of the thallium pyrochlores are presumed to be dependent on the reaction conditions, and the compositions expected for this system are as follows: (i) $Tl_2Ru_2O_{7-\delta}$ (oxygen deficiency), (ii) $Tl_{2-\delta'}Ru_2O_7$ (thallium deficiency), and (iii) $Tl_{2-\delta'}Ru_2O_{7-\delta}$ (both oxygen and thallium deficiencies). The following reaction conditions are therefore studied.

(i) Oxygen deficiency: Ru metal was used as a starting material to keep a reducing condition in a high-pressure vessel. The oxidation states expected are Tl^{3+}, Tl^{+}, Ru^{4+}, and Ru^{3+}.

(ii) No deficiency in the structure (stoichiometric pyrochlore): High oxygen pressure was applied using $KClO_4$ to minimize the amount of oxygen deficiency. The oxidation states expected are Tl^{3+} and Ru^{4+}.

(iii) Thallium deficiency: Tl_2O_3 and RuO_2 were used as starting materials with a Tl/Ru ratio < 1.0. High oxygen pressure was applied with $KClO_4$. The oxidation states expected are Tl^{3+}, Ru^{5+}, and Ru^{4+}.

(iv) Thallium and oxygen deficiencies: The starting materials, Tl_2O_3 and RuO_2, were used with a Tl/Ru ratio < 1.0. The oxidation states expected are Tl^{3+} and Ru^{4+}.

TABLE 1
Materials Data for $Tl_{2-\delta}Ru_2O_{7-\delta}$

Nominal compositions	Reaction conditions	Lattice parameter a/Å	Impurity phases
$Tl_2Ru_2O_{6.5}$[a]	1 GPa, 1173 K	10.18950(10)	RuO_2, Tl_2O_3
$Tl_{1.8}Ru_2O_{6.5}$[a]	1 GPa, 1173 K	10.18721(19)	RuO_2
$Tl_2Ru_2O_7$[b]	1 GPa, 1173 K	10.18618(10)	—
$Tl_{1.9}Ru_2O_{6.85}$[b,h]	1 GPa, 1173 K	10.18492(19)	RuO_2
$Tl_{1.8}Ru_2O_{6.7}$[b]	5 GPa, 1173 K	10.18261(15)	RuO_2
$Tl_{1.7}Ru_2O_{6.55}$[b]	1 GPa, 1173 K	10.1854(2)	RuO_2
$Tl_2Ru_2O_7$[c]	1 GPa, 1173 K	10.18425(17)	RuO_2[d]
$Tl_{1.95}Ru_2O_7$[c]	1 GPa, 1173 K	10.1850(2)	RuO_2
$Tl_{1.83}Ru_2O_7$[c]	1 GPa, 1173 K	10.1847(2)	RuO_2
$Tl_{1.8}Ru_2O_7$[c,i]	1 GPa, 1173 K	10.1822(2)	RuO_2
$Tl_2Ru_{1.8}O_7$[c]	1 GPa, 1173 K	10.1840(2)	RuO_2, Tl_2O_3
$Tl_2Ru_2O_7$[e]	0.3 GPa, 973 K	10.20(1)	—
$Tl_2Ru_2O_7$[e]	3 GPa, 1173 K	10.188	TlCl, RuO_2
$Tl_2Ru_2O_7$[e]	0.3 GPa, 1223 K	10.1863	Tl_2O_3, RuO_2
$Tl_2Ru_2O_7$[e]	3 GPa, 1173 K	10.174	TlCl, RuO_2
$Tl_2Ru_2O_7$[e]	0.3 GPa, 1223 K	10.188	Tl_2O_3, RuO_2
$Tl_2Ru_2O_7$[e]	0.3 GPa, 1223 K	10.188	Tl_2O_3, TlCl, RuO_2
$Tl_2Ru_2O_7$[f,g]	ambient, 773 K	10.2116(10)	RuO_2
$Tl_2Ru_2O_{6.71}$[f,g]	ambient, 1173 K	10.2008(9)	—

[a]High-pressure synthesis using Ru metal as a starting material (reducing conditions).
[b]High-pressure synthesis.
[c]High-oxygen-pressure synthesis using $KClO_4$ as an oxidizing agent.
[d]Very small amount of RuO_2 was detected.
[e]After Jarrett *et al.* (5).
[f]Compositions determined by neutron diffraction measurements.
[g]After Kanno *et al.* (13).
[h]The composition, $Tl_2Ru_2O_{6.96}$, was determined by the neutron diffraction measurement in the present study.
[i]The composition, $Tl_2Ru_2O_7$, was determined by the neutron diffraction measurement in the present study.

Table 1 summarizes the materials data for $Tl_{2-\delta}Ru_2O_{7-\delta}$ synthesized in the present study together with those reported previously (5, 13). The compositions indicated in Table 1 are taken from the starting compositions of the syntheses (nominal compositions) and the oxygen compositions are written as 7.0 when the high oxygen pressure was applied with $KClO_4$. Among these samples, the compositions of "$Tl_{1.8}Ru_2O_7$" and "$Tl_{1.9}Ru_2O_{6.85}$" were determined by neutron diffraction data in the present study as $Tl_2Ru_2O_7$ and $Tl_2Ru_2O_{6.96}$, respectively. Impurity phases such as RuO_2 and Tl_2O_3 were always observed except for the stoichiometric starting composition, $Tl_2Ru_2O_7$. The lattice parameters varied with the reaction conditions as indicated previously (5). Reducing reaction conditions with Ru metal as a reactant have led to slightly larger lattice parameters. This is consistent with the previous results that the samples synthesized at 1173 K under ambient pressure have the composition $Tl_2Ru_2O_{6.71}$ with larger lattice parameters than those synthesized at high pressures. Oxygen vacancies in the O(2) sites might lead to larger lattice parameters. On the other hand, the oxidizing conditions using $KClO_4$ led to samples with slightly smaller lattice parameters.

3.2. Electrical Properties

Figure 1 shows temperature dependence of the resistivity for $Tl_2Ru_2O_{7-\delta}$ synthesized at high pressures. The electrical properties are divided into three categories: (i) metallic, (ii) metallic-to-semiconducting transition around 40 K, and (iii) metallic–semiconducting transition around 120 K. These categories correspond to the samples synthesized under reducing high-pressure conditions, high-pressure conditions, and high-oxygen-pressure conditions, respectively. The samples synthesized in the reduced conditions (nominal compositions, $Tl_2Ru_2O_{6.5}$ and $Tl_{1.8}Ru_2O_{6.5}$) showed metallic behavior with low resistivity values. The behavior is similar to that observed for the high-temperature phase, $Tl_2Ru_2O_{6.71}$, obtained at the atmospheric synthesis condition (13). The samples obtained under a pressure of 1–5 GPa without oxidizing or reducing agents (nominal compositions, $Tl_2Ru_2O_7$, $Tl_{1.9}Ru_2O_{6.75}$, $Tl_{1.8}Ru_2O_{6.7}$, $Tl_{1.7}Ru_2O_{6.55}$) showed a slope change in the resistivity curves around 40 K which corresponds to a metallic-to-semiconducting transition. The samples obtained under a high oxygen pressure (nominal compositions, $Tl_2Ru_2O_7$, $Tl_{1.83}Ru_2O_7$, $Tl_{1.8}Ru_2O_7$) showed a metallic–semiconducting transition around 120 K accompanying a drastic resistivity increase of 2 orders of magnitude.

3.3. Magnetic Properties

Magnetization (M) was measured as a function of applied field (H) at several fixed temperatures and also as a function of temperature at fixed fields. The magnetization was measured after cooling in zero field, and then measured again down to 4 K in the applied magnetic field. Figure 2 shows a typical temperature dependence of M/H measured from 4 to 300 K at 1 kOe for the sample synthesized at a high oxygen pressure (nominal composition, $Tl_{1.8}Ru_2O_7$) and at a high pressure (nominal composition, $Tl_{1.9}Ru_2O_{6.85}$). For "$Tl_{1.8}Ru_2O_7$," almost temperature independent magnetization was observed from 300 to 120 K, and an abrupt decrease in the magnetization was found at the metallic–semiconducting transition. A small anomaly was also observed around 40 K with a large increase in the magnetization at low temperatures.

On the other hand, "$Tl_{1.9}Ru_2O_{6.85}$" showed a large history dependence in the range $5\,K \leq T \leq 40\,K$. The field cooled (fc) M/H is much larger than the zero field cooled (zfc) M/H, and the cusp was observed at 40 K for the zfc M/H curve. Isothermal magnetization data at 5 K are

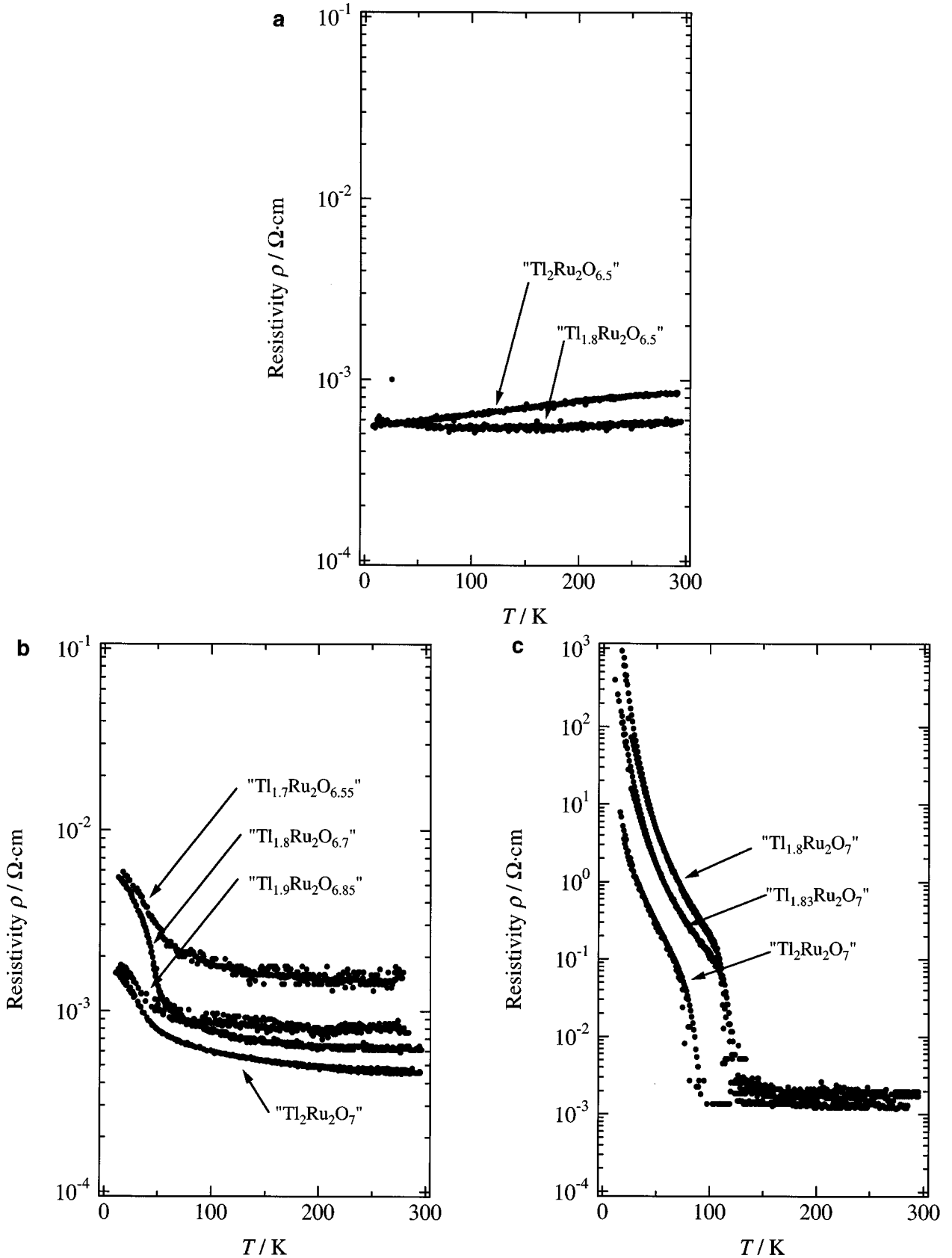

FIG. 1. Temperature dependence of resistivity for the thallium pyrochlores. The nominal compositions are indicated in the figure.

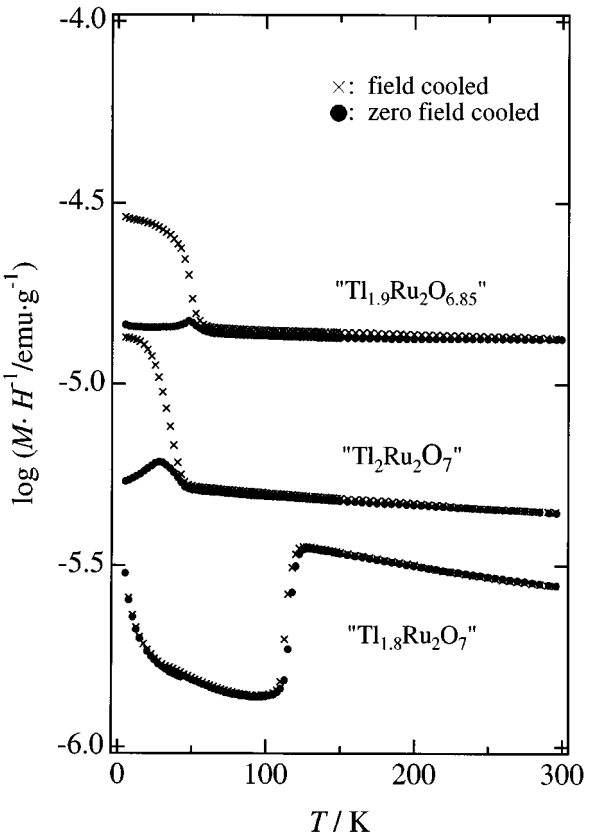

FIG. 2. Temperature dependence of magnetization M/H for the thallium pyrochlores. The nominal compositions are indicated in the figure.

shown in Fig. 3 for "$Tl_{1.8}Ru_2O_7$" and "$Tl_{1.9}Ru_2O_{6.85}$." (The compositions of these samples were determined by neutron diffraction measurements to be $Tl_2Ru_2O_7$ and $Tl_2Ru_2O_{6.96}$, respectively.)

Figure 4 summarizes the starting compositions, reaction conditions, and their electrical properties of the reaction products. The nominal compositions are indicated in the figure. The reducing conditions led to metallic properties and slightly larger lattice parameters which are shown in Table 1. However, no significant difference in lattice parameters was observed between the samples obtained at high pressure and high oxygen pressure (see Table 1).

The samples synthesized under high oxygen pressure showed the metallic–semiconducting transition around 100–125 K with an abrupt magnetization drop at the transition temperature. A small magnetization anomaly was also observed around 40 K. This anomaly might be caused either by another magnetic interaction or by an impurity phase with less oxygen content. The samples synthesized under high pressure showed the metallic-to-semiconducting change around 30–50 K with a large history dependence in the magnetization curves which is similar to a spin-glass-like behavior or canted antiferromagnet. The oxygen content might affect their electrical and magnetic properties. On the other hand, thallium deficiency, if it exists in the reaction products according to the nominal compositions, might not affect their physical properties.

3.4. Structure Refinements

To clarify the compositions and structures of the phases obtained in the present study, the structure parameters were refined using neutron powder diffraction data for the samples, "$Tl_{1.9}Ru_2O_{6.85}$" and "$Tl_{1.8}Ru_2O_7$" which were synthesized under high pressure and high oxygen pressure, respectively. Intensity data for interplanar spacings between 0.67 and 4.0 Å were used for Rietveld analysis.

Structural parameters were refined with space group $Fd\bar{3}m$ using a structural model, Tl at 16d ($\frac{1}{2}$, $\frac{1}{2}$, $\frac{1}{2}$), Ru at 16c (0, 0, 0), and O(1) at 48f (x, $\frac{1}{8}$, $\frac{1}{8}$) with $x \approx 0.32$, and O(2) at 8b ($\frac{3}{8}$, $\frac{3}{8}$, $\frac{3}{8}$). The site occupation parameters, g, of the Tl, Ru, and O(2) sites were also refined; no significant deviation from the stoichiometric composition ($g = 1$) was observed for the Tl or Ru sites in both samples. In the final refinement cycle, anisotropic thermal parameters were assigned for all the sites. No correction was made for preferred orientation. Table 2 lists final R factors, lattice, and structural parameters with their estimated standard deviations in parentheses. Table 3 gives interatomic distances and bond angles calculated with ORFFE (16). Figure 5 illustrates the profile fit and difference patterns for both samples. For the refinement of the high-oxygen-pressure phase (a nominal composition, "$Tl_{1.8}Ru_2O_7$"), the g value at the O(2) sites exceeded 1.00; thus the g value was fixed at 1. The occupancy at the O(2) site was determined to be 0.96(3) ($Tl_2Ru_2O_{6.96}$) for the samples synthesized under a high pressure (a nominal composition, "$Tl_{1.9}Ru_2O_{6.85}$").

The oxygen content, δ, in $Tl_2Ru_2O_{7.0-\delta}$ was determined in the present study for the phases which were synthesized under high pressure ($Tl_2Ru_2O_{6.96}$) and high oxygen pressure ($Tl_2Ru_2O_7$). On the other hand, the thallium site is fully occupied by Tl, despite the change in the starting compositions. The oxygen nonstoichiometry in the thallium pyrochlores varies depending on the synthesis conditions, and the ambiguity in physical properties reported previously (5) might be caused by the difficulties in the control of oxygen nonstoichiometry when reactions at atmospheric pressure are used.

The results on the oxygen contents are summarized as follows. (i) The high-temperature phase synthesized under atmospheric pressure has a large amount of oxygen vacancy of 0.29(2) (13). (ii) The stoichiometric composition with respect to the oxygen content $\delta = 0$ is obtained by applying high oxygen pressure. (iii) The high-pressure phase has a small amount of vacancy of 0.04(3). (iv) The low-temperature phase synthesized under atmospheric pressure is stoichiometric, $\delta = 0$ (13).

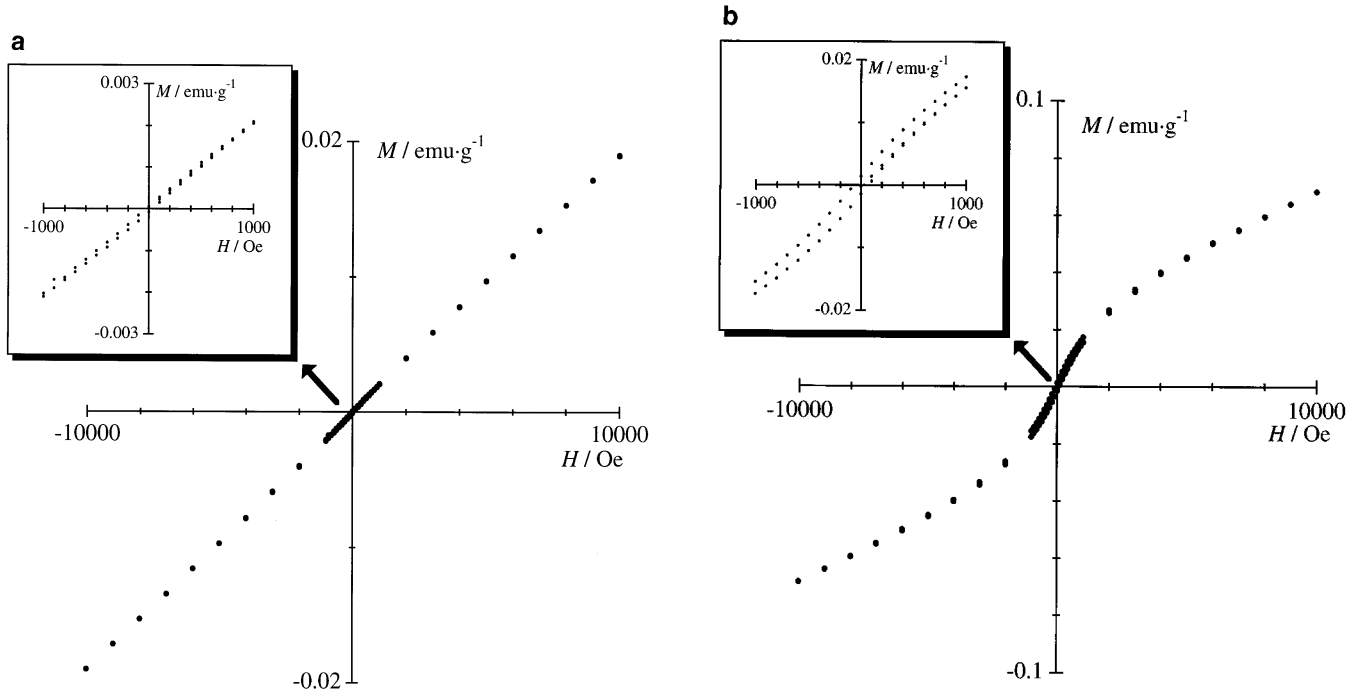

FIG. 3. Isothermal magnetization data at 5 K for "$Tl_{1.8}Ru_2O_7$" (a) and "$Tl_{1.9}Ru_2O_{6.85}$" (b).

The oxygen contents of the two thallium pyrochlores, high-oxygen-pressure phase ($Tl_2Ru_2O_{7.000(6)}$) and high-pressure phase ($Tl_2Ru_2O_{6.951(6)}$) were also confirmed by our neutron diffraction experiments at 100 K, which will be published elsewhere.

3.5. Structure–Property Relationship in the Pyrochlores

The relationship between the physical properties and the oxygen content is now clarified. (i) The high-temperature phase having oxygen nonstoichiometry, $Tl_2Ru_2O_{6.71}$, is metallic. (ii) The high oxygen pressure phase with the stoichiometric composition, $Tl_2Ru_2O_7$, showed the metallic–semiconducting transition at 120 K. The small magnetization anomaly at 40 K might correspond to the spin-glass-like behavior which is observed for $Tl_2Ru_2O_{6.96}$. (iii) A small amount of oxygen vacancy in the structures, for example, in $Tl_2Ru_2O_{6.96}$ synthesized under high pressure led only to a spin-glass-like behavior with a resistivity increase at the transition temperature around 40 K. (iv) The stoichiometric $Tl_2Ru_2O_7$ synthesized under atmospheric pressure is semiconducting.

Electron microprobe analysis of the samples, $Tl_2Ru_2O_7$ (ii), $Tl_2Ru_2O_{6.96}$ (iii), and $Tl_2Ru_2O_7$ (iv) indicated the Tl : Ru ratio of 1 : 1 within their accuracy. The results are consistent with the neutron diffraction results, and the variation of the properties is mainly dependent on the oxygen content. However, the semiconducting property of the low-temperature phase $Tl_2Ru_2O_7$ is rather difficult to understand. In the present study, the magnetization of this phase was measured using the sample synthesized at 773 K in a sealed tube (13). Temperature dependence of the magnetization is shown in Fig. 6. Magnetization change was observed near 120 K which corresponds to the metallic–semiconducting transition of the high-oxygen-pressure phase, $Tl_2Ru_2O_7$. The difference between fc and zfc magnetization at $T < 40$ K corresponds to the spin-glass-like behavior for $Tl_2Ru_2O_{6.96}$, and was also observed for $Tl_2Ru_2O_7$. The results indicate two different kinds of stoichiometric phases, one is the high-oxygen-pressure phase with the metallic–semiconducting transition, and the other is the low-temperature phase with semiconducting property synthesized at ambient pressure.

To confirm the two modifications of the stoichiometric $Tl_2Ru_2O_7$, conversion between the high-pressure phase and ambient-pressure phase was examined. The sample ($Tl_2Ru_2O_7$ high-oxygen-pressure phase showing the transition at 120K) was sealed in a quartz tube under vacuum and annealed at 550°C for 96 h. The resistivity measurement of this phase after this treatment indicated only a slope change in the resistivity curve around 120 K, and the drastic resistivity change disappeared. The semiconducting $Tl_2Ru_2O_7$ (low-temperature phase synthesized at ambient-pressure conditions) was treated at 1 GPa and 900°C. The resistivity measurement indicated that the metallic–semiconducting transition appeared around 80 K

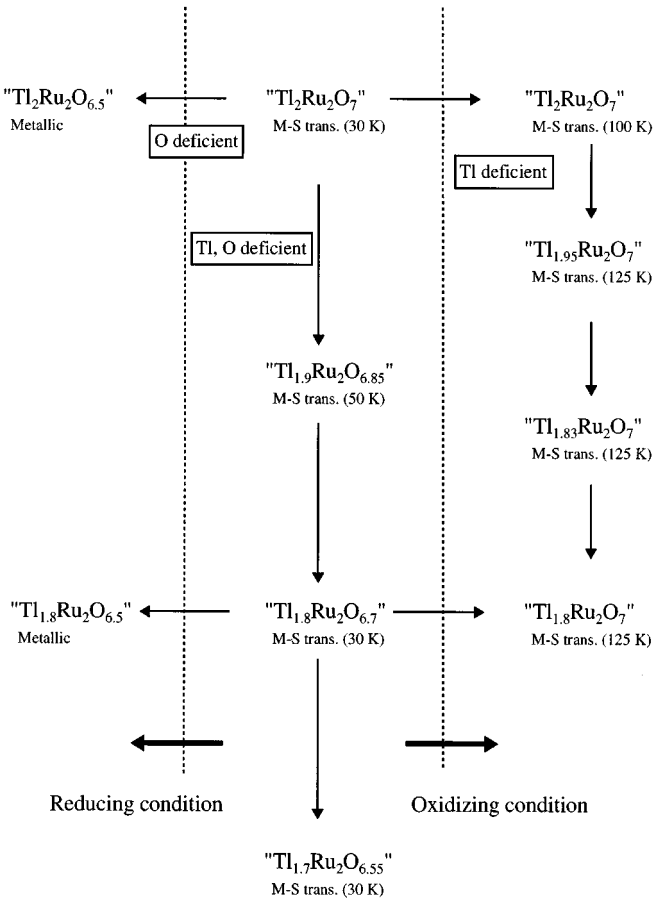

FIG. 4. Relationship between the starting compositions and electrical properties; "M–S trans," Metallic–semiconducting transition. Transition temperatures are indicated in the parentheses. Nominal compositions are indicated in the figure.

with a resistivity change of 1 order of magnitude. These results confirmed that both the high-pressure phase and ambient-pressure phase exist for $Tl_2Ru_2O_7$, and converting from high-pressure phase to ambient-pressure phase is reversible.

The diffraction experiments of the low-temperature ambient pressure phase, $Tl_2Ru_2O_7$, indicated rather broad X-ray and neutron diffraction peaks (see Fig. 2 in Ref. (13)) which might be caused by an inhomogeneity in the structure. The electrical properties might be affected by the inhomogeneity or local disordering in the structure, and this could be a reason for the semiconducting behavior. Further studies on this low-temperature phase are still necessary based on the local structure analysis such as TEM observations and EXAFS measurements.

To clarify the relations between the structures and physical properties, the bond distances and angles are summarized for the four typical samples with different synthesis conditions, (i) $Tl_2Ru_2O_{6.71}$ (high-temperature phase having

TABLE 2
Rietveld Refinement results for $Tl_2Ru_2O_{7-\delta}$

(a) $Tl_2Ru_2O_{6.96}$ synthesized under high pressure conditions

Atom	Site	g	x	y	z	B_{eq} (Å^2)
Tl	16*d*	1	$\frac{1}{2}$	$\frac{1}{2}$	$\frac{1}{2}$	1.46
Ru	16*c*	1	0	0	0	1.34
O(1)	48*f*	1	0.3247(4)[a]	$\frac{1}{8}$	$\frac{1}{8}$	1.61
O(2)	8*b*	0.96(3)	$\frac{3}{8}$	$\frac{3}{8}$	$\frac{3}{8}$	1.45

Atom	U_{11} (Å^2)[b]	U_{22} (Å^2)	U_{33} (Å^2)	U_{12} (Å^2)	U_{13} (Å^2)	U_{23} (Å^2)
Tl	0.0185(14)	$=U_{11}$	$=U_{12}$	−0.0006(16)	$=U_{12}$	$=U_{12}$
Ru	0.0170(14)	$=U_{11}$	$=U_{12}$	0.000(2)	$=U_{12}$	$=U_{12}$
O(1)	0.023(2)	0.0189(16)	$=U_{22}$	0	0	0.04(2)
O(2)	0.018(4)	$=U_{11}$	$=U_{12}$	0	0	0

$a = 10.1831(2)$Å, $R_{wp} = 6.86$, $R_p = 5.36$, $S = R_{wp}/R_e = 1.12$, $R_I = 3.74$, and $R_F = 3.04$

(b) $Tl_2Ru_2O_7$ synthesized under high-oxygen-pressure conditions

Atom	site	g	x	y	z	B_{eq} (Å^2)
Tl	16*d*	1	$\frac{1}{2}$	$\frac{1}{2}$	$\frac{1}{2}$	1.46
Ru	16*c*	1	0	0	0	1.28
O(1)	48*f*	1	0.3256(4)	$\frac{1}{8}$	$\frac{1}{8}$	1.68
O(2)	8*b*	1	$\frac{3}{8}$	$\frac{3}{8}$	$\frac{3}{8}$	1.63

Atom	U_{11} (Å^2)[c]	U_{22} (Å^2)	U_{33} (Å^2)	U_{12} (Å^2)	U_{13} (Å^2)	U_{23} (Å^2)
Tl	0.0184(16)	$=U_{11}$	$=U_{12}$	−0.0012(17)	$=U_{12}$	$=U_{12}$
Ru	0.0162(15)	$=U_{11}$	$=U_{12}$	0.000(2)	$=U_{12}$	$=U_{12}$
O(1)	0.024(2)	0.0199(16)	$=U_{22}$	0	0	0.04(2)
O(2)	0.021(3)	$=U_{11}$	$=U_{12}$	0	0	0

$a = 10.1865(2)$Å, $R_{wp} = 9.55$, $R_p = 6.96$, $S = R_{wp}/R_e = 1.23$, $R_I = 3.66$, and $R_F = 3.08$

Structural parameters for RuO_2[c]

Atom	Site	g	x	y	z	B (Å^2)
Ru	2*a*	1	0	0	0	1.4(5)
O	4*f*	1	0.309(2)	$=x$	0	0.5(3)

$a = 4.4890(2)$Å, $c = 3.1049(4)$Å, $R_I = 8.61$, and $R_F = 5.73$

[a] Numbers in parentheses are estimated standard deviations of the last significant digit.

[b] The form of the anisotropic temperature factor is

$$\exp[-2\pi^2(h^2a^{*2}U_{11} + k^2b^{*}U_{22} + l^2c^{*2}U_{33} + 2hka^{*}b^{*}U_{11} + 2hla^{*}c^{*}U_{13} + 2klb^{*}c^{*}U_{23})].$$

[c] Refinement using space group $P4_2/mnm$.

TABLE 3
Interatomic Distances (Å) and Bond Angles (deg) for $Tl_2Ru_2O_{7-\delta}$[a]

Phase		$Tl_2Ru_2O_{6.96}$	$Tl_2Ru_2O_7$
		Interatomic distances	
$Tl–O(1)^{i}$	(×6)	2.535(3)	2.530(3)
Tl–O(2)	(×2)	2.2047(1)	2.2054(1)
$Ru–O(1)^{ii}$	(×6)	1.9543(17)	1.9586(18)
		Bond angles	
$Ru^{iii}–O(1)–Ru^{iv}$		134.2(2)	133.7(2)
$Tl^{v}–O(1)–Tl^{vi}$		90.48(14)	90.78(15)
$Tl^{v}–O(1)–Tl^{vii}$		109.4712	109.4712
$O(1)^{ii}–Ru–O(1)^{viii}$		94.75(15)	95.09(17)

[a]Coordinate triplets: (i) $x, y+\frac{1}{2}, z+\frac{1}{2}$; (ii) $x-\frac{1}{4}, y+\frac{1}{4}, -z$; (iii) $-x+\frac{1}{4}, -y+\frac{1}{4}, z$; (iv) $-x+\frac{1}{4}, y, -z+\frac{1}{4}$; (v) $x, -y+\frac{3}{4}, -z+\frac{3}{4}$; (vi) $x, y-\frac{1}{2}, z-\frac{1}{2}$; (vii) $-x+\frac{3}{4}, y, -z+\frac{3}{4}$; (viii) $-z, x-\frac{1}{4}, y-\frac{1}{4}$.

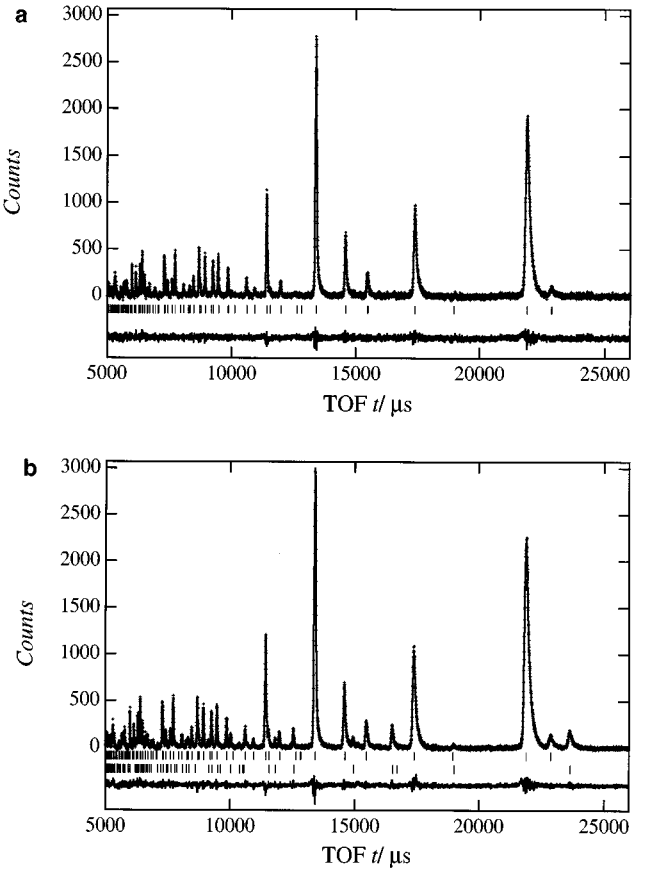

FIG. 5. Observed, calculated, and difference plots for the neutron Rietveld analysis for $Tl_2Ru_2O_{6.96}$ (a) and $Tl_2Ru_2O_7$ (b). The refinement of $Tl_2Ru_2O_7$ (b) was carried out using the two-phase model with RuO_2. The solid line depicts calculated intensities, the overlying dots the observed intensities, and Δy_i the difference between the observed and calculated intensities.

oxygen nonstoichiometry), (ii) $Tl_2Ru_2O_7$ (high-oxygen-pressure phase with the stoichiometric composition), (iii) $Tl_2Ru_2O_{6.96}$ (high-pressure phase with small amount of oxygen vacancy), (iv) $Tl_2Ru_2O_7$ (low-temperature phase at ambient-pressure conditions). For the low-temperature semiconducting phase (iv), the average structure which was determined by the neutron diffraction experiments (13) is considered in the present study. Figure 7 shows temperature dependence of electrical resistivities of these phases. Each sample shows typical behavior of (i) metallic, (ii) metallic–semiconducting transition at 120 K, (iii) metallic-to-semiconducting change at 50 K, and (iv) semiconducting behavior.

Like the cubic-perovskite structure, the pyrochlores $A_2B_2O_6O'$ have a BO_3 array of corner-shared octahedra, but the *B*–O–*B* angles are reduced from 180 to about 130°. Reduction of the *B*–O–*B* angles from 180° reduces the *B*–O–*B* overlap integrals; the electrical properties of the pyrochlores might thus be affected by a small change in the *B*–O–*B* angles. Figure 8 shows the relationship between the bond distances and bond angles of four samples indicated above, (i)–(iv). With increasing Ru–O(1) distances, the Tl–O(1) distance decreases, the Ru–O(1)–Ru angle decreases, and two O(1)–Ru–O(1) angles split from 90°. The increase in the Ru–O(1) bond lengths leads to the distortion of RuO_6 octahedra and to the reduction of Ru–O(1)–Ru angles, which tends to localize electrons due to the reduced Ru–O(1) interaction.

The pyrochlore structure is viewed as being made up of two networks, $(Tl_2O)_\infty$ and $(RuO_3)_\infty$, which interpenetrate with each other. The bridging oxide ions, O(1), are connected to both Tl and Ru ions, and the Tl–O(1) bond strength might strongly affect the Ru–O(1) bond. These two interactions are competitive; the stronger the Tl–O(1) bond, the weaker the Ru–O(1) bond. The fact that the Tl–O(1) distance decreases with increasing Ru–O(1) distance corresponds to the change from semiconducting to metallic character, through the metallic–semiconducting transition.

The relationship between the electrical properties and the structures has been reported for the $Bi_{2-x}Ln_xRu_2O_7$ and $Pb_{2-x}Ln_xRu_2O_{7-\delta}$ (*Ln* = Pr–Lu, Y) solid solutions (10–12). The resistivity increases with *x*, and the metallic property changes to semiconducting between $x = 1.2$ and 1.4. With increasing *Ln* content, the Ru–O(1) bond lengths increase, the distortion of the RuO_6 octahedra increases, and the bend in the RuO_6 zigzag chains increases from $x = 0$ to 2.0. These structural changes are quite similar to those found in the thallium pyrochlores. Figure 9 summarizes the Ru–O(1) bond distances and the Ru–O(1)–Ru angles for the Ru-containing pyrochlores. The metallic region is obviously separated from the semiconducting region; the compounds with Ru–O(1) distances of 1.94–1.97 Å and Ru–O(1)–Ru

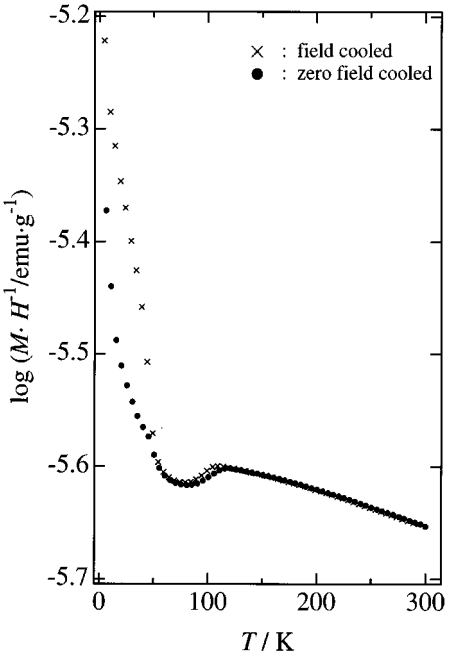

FIG. 6. Temperature dependence of magnetization M/H for the thallium pyrochlores, $Tl_2Ru_2O_7$, synthesized at 773 K and ambient-pressure.

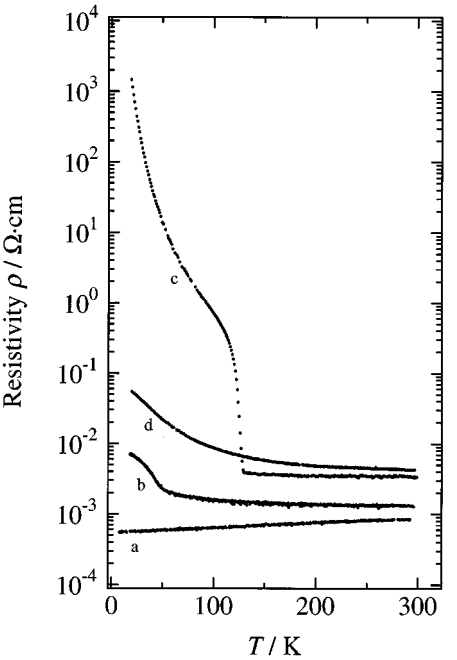

FIG. 7. Temperature dependence of the resistivity for the thallium pyrochlores. (a) $Tl_2Ru_2O_{6.71}$: high-temperature phase (HT), metallic: (b) $Tl_2Ru_2O_{6.96}$: high-pressure phase, resistivity change around 50 K. (c) $Tl_2Ru_2O_7$: high-oxygen-pressure phase, metallic–semiconducting transition at 120 K. (d) $Tl_2Ru_2O_7$: low-temperature phase (LT), semiconducting.

angles of 134–139° show metallic behavior, and those with Ru–O(1) distances of 1.97–2.00 Å and Ru–O(1)–Ru angles of 129–134° show semiconducting behavior. The bond distances and bond angles determined for $Tl_2Ru_2O_{7-\delta}$ correspond to the borderline between metallic and semiconducting behavior. Recently, the importance of the Ru–O–Ru angle was also confirmed based on neutron diffraction data on $Ln_2Ru_2O_7$ (18). They indicated that the angles greater than 133° are necessary to facilitate metallic conductivity, which is consistent with the present results.

Figure 10 shows the relations between ionic radii of A ions (17) and A–O(1), A–O(2), and the average of eight A–O distances in the ruthenium pyrochlores. The data are taken from our previous X-ray Rietveld refinement results (10, 11) and also from the recent results on neutron diffraction experiments (18). The bond distances obtained from the X-ray and neutron diffraction experiments are consistent with each other except the bismuth pyrochlore. This might be caused by the difference in the sample stoichiometry; the sample used for the structure analysis using neutron diffraction contains O(2) deficiency and the composition was $Bi_2Ru_2O_{6.92}$ (19). The Pb–O distances are also shorter than the value expected from other lanthanum series, which might be caused by the different valence, $Pb^{2.5+}$, and the oxygen deficiency (20).

In the stoichiometric pyrochlores ($A_2Ru_2O_7$, A = Y, Dy, Gd, Sm, Nd, Pr, Bi, Tl), the A–O distances increase with increasing ionic radii of the lanthanum ions from Y to Pr, and the Bi–O distances obtained by the X-ray data are consistent with those expected from the extrapolation from Y to Pr. The dashed line, A–O(average), is obtained from the sum of the ionic radii of lanthanum ions and oxygen ions and the line is consistent with the A–O(average) plots determined from the X-ray and neutron diffraction experiments. However, the Tl–O distances significantly deviate from the values expected from the relation. This indicates that the ionic radii used for thallium (17) is too short in the pyrochlore structure and a reasonable value for Tl^{3+}(VIII) is estimated from this figure to be 1.08–1.09 Å.

3.6. Phase Transition at Low Temperatures

To clarify the phase transition for $Tl_2Ru_2O_{7-\delta}$ at low temperatures, X-ray diffraction was measured at low temperatures for the samples showing metallic–semiconducting transition at 120 K ($Tl_2Ru_2O_{7.0}$) and 40 K ($Tl_2Ru_2O_{6.96}$). Figure 11 shows the temperature dependence of lattice parameters for $Tl_2Ru_2O_7$ and $Tl_2Ru_2O_{6.96}$ from 10 to 300 K. A discontinuous change in the lattice parameter curve was observed for $Tl_2Ru_2O_7$ at the transition temperature. Figure 12 shows the X-ray diffraction patterns at 290 and 105 K for $Tl_2Ru_2O_7$. The pattern at 105 K shows small reflections which are indexed by a cubic cell with the lattice

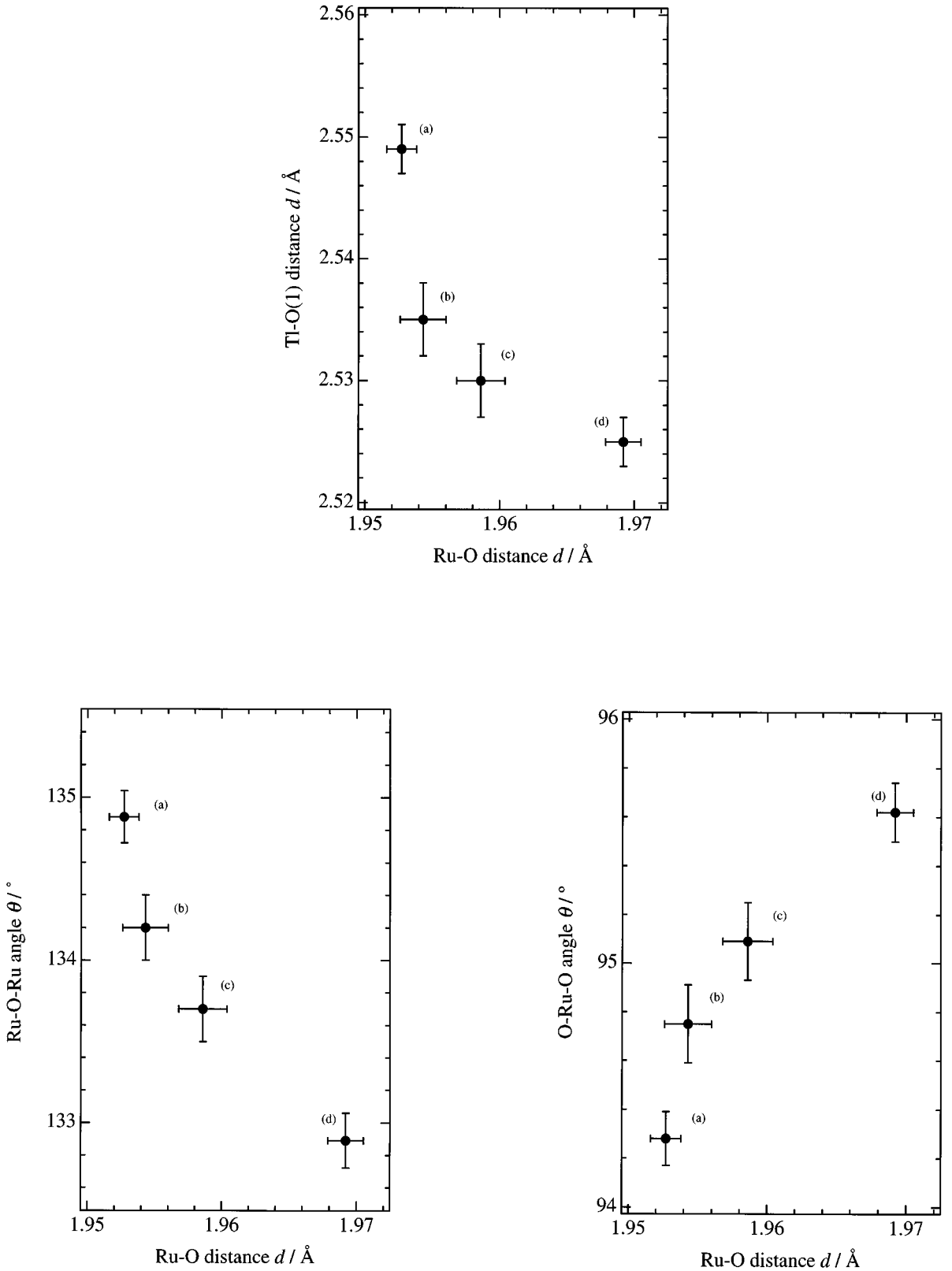

FIG. 8. Relations between the Ru–O distances, Tl–O(1) distances, Ru–O(1)–Ru angles, and O–Ru–O angles. (a) $Tl_2Ru_2O_{6.71}$: high-temperature phase, metallic; (b) $Tl_2Ru_2O_{6.96}$: high-pressure phase, resistivity change around 50 K. (c) $Tl_2Ru_2O_7$: high-oxygen-pressure phase, metallic–semiconducting transition at 120 K. (d) $Tl_2Ru_2O_7$: low-temperature phase, semiconducting.

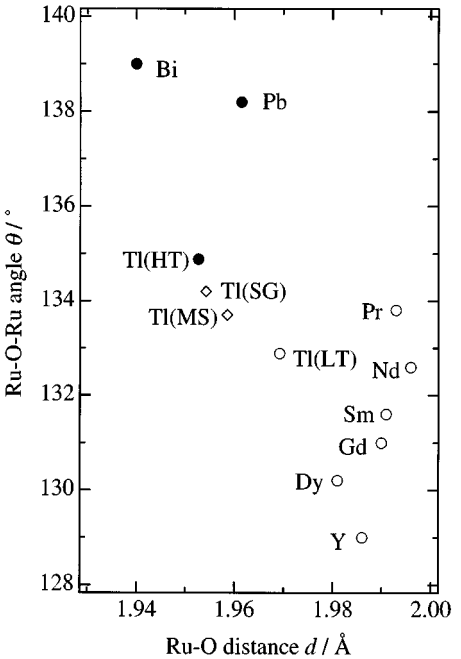

FIG. 9. Relations between the Ru–O bond distances and the Ru–O–Ru angles in $A_2Ru_2O_{7-\delta}$. (●) Samples showing metallic property; (○) samples showing semiconducting property; (◇) samples showing metallic–semiconducting transition; Tl(HT), $Tl_2Ru_2O_{6.71}$; Tl(LT), $Tl_2Ru_2O_7$, low-temperature phase; Tl(SG), $Tl_2Ru_2O_7$, high-pressure phase; Tl(MS), $Tl_2Ru_2O_7$, high-oxygen-pressure phase.

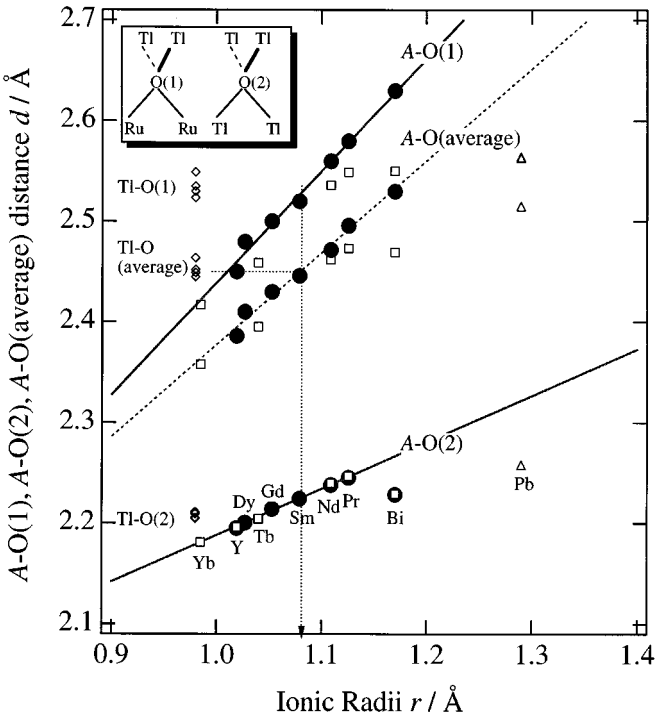

FIG. 10. Relations between ionic radii and *A*–O bond distances. Bond distances are taken from X-ray (10, 11) (●) and neutron [this study (◇); Ref. (2) (△); and Ref. (18) (□)] diffraction experiments. Straight lines in the *A*–O(1) and *A*–O(2) distances indicate the least-squares fit of the bond distances from $A_2Ru_2O_7$ (A = Yb–Pr, Y). The dashed line is calculated from the sum of the ionic radii of A^{3+}(VIII) ions and O^{2-}(IV) ions.

parameter, $a = 10.176$ Å, similar to that of the room temperature phase. However, no extinction rules were observed. The transition of the stoichiometric $Tl_2Ru_2O_7$ was first-order accompanying the symmetry change, which is consistent with the hysteresis observed in the electrical and magnetic properties at the transition temperature of 120 K. For the slightly nonstoichiometric $Tl_2Ru_2O_{6.96}$, no significant anomaly in the lattice parameter curve was observed at the transition, which is an indication of a higher order transition.

In the pyrochlore structure, the 16*d* and 16*c* sites in space group $Fd\bar{3}m$, form a three-dimensional network of perfect corner-sharing tetrahedra. It has been recognized that a magnetic sublattice with this symmetry will give rise to fully frustrated interactions in three dimensions if the exchange interaction between ions is predominantly antiferromagnetic. Behavior related to the spin-glass state has been reported for $Y_2Mo_2O_7$ (21), $Tb_2Mo_2O_7$ (22), and the solid solution series, $Y_{1-x}La_xMo_2O_7$ (23). The frustration behavior of $Tl_2Ru_2O_7$ is the first example in the Ru-containing pyrochlores. A low-temperature neutron diffraction study is currently underway in order to understand the metallic–semiconducting transition and the spin frustration behavior.

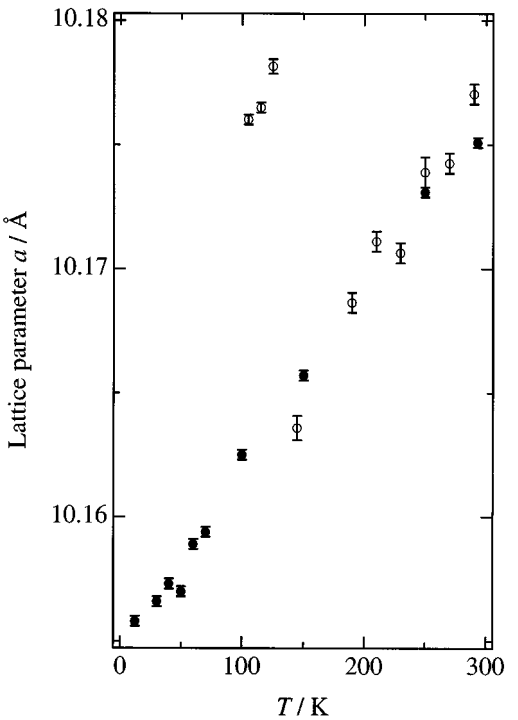

FIG. 11. Temperature dependence of the lattice parameters for $Tl_2Ru_2O_7$ (○) and $Tl_2Ru_2O_{6.96}$ (●).

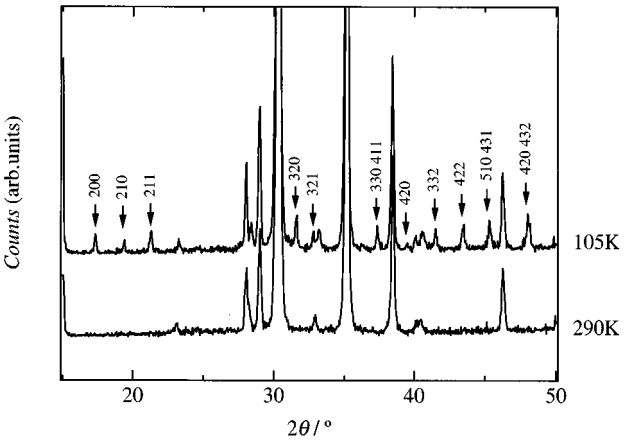

FIG. 12. X-ray diffraction patterns for $Tl_2Ru_2O_7$ at 105 and 290 K.

REFERENCES

1. R. J. Bouchard and J. L. Gillson, *Mater. Res. Bull.* **6,** 69 (1971).
2. J. M. Longo, P. M. Raccah, and J. B. Goodenough, *Mater. Res. Bull.* **4,** 191 (1969).
3. R. Aleonard, A. F. Berthand, M. C. Montomry, and R. Pauthenet, *J. Appl. Phys.* **33,** 1205 (1962).
4. A. W. Sleight and R. J. Bouchard, *in* "Solid State Chemistry, Proceedings of the 5th Materials Research Symposium, July 1972," p. 227. NBS Spec. Publ. 364, NBS, Washington, DC, 1975.
5. H. S. Jarrett, A. W. Sleight, J. F. Weiher, J. L. Gillson, C. G. Frederick, G. A. Jones, R. S. Swingle, D. Swartzfager, J. E. Gulley, and P. C. Hoell, "Valence Instabilities and Related Narrow-Band Phenomena" (R. D. Parks, Ed.), p. 545. Plenum, New York, 1977.
6. J. B. Goodenough, A. Hamnett, and D. Telles, "Localization and Metal–Insulator Transition" (H. Fritzshe and D. Adler, Eds.), p. 161. Plenum, New York, 1985.
7. P. A. Cox, J. B. Goodenough, P. J. Tavener, D. Telles, and R. G. Egdell, *J. Solid State Chem.* **62,** 360 (1986).
8. P. A. Cox, R. G. Egdell, J. B. Goodenough, A. Hamnett, and C. C. Naish, *J. Phys. C* **16,** 6221 (1983).
9. W. Y. Hsu, R. V. Kasowski, T. Miller, and T.-C. Chiang, *Appl. Phys. Lett.* **52,** 792 (1988).
10. R. Kanno, Y. Takeda, T. Yamamoto, Y. Kawamoto, and O. Yamamoto, *J. Solid State Chem.* **102,** 106 (1993).
11. T. Yamamoto, R. Kanno, Y. Takeda, O. Yamamoto, Y. Kawamoto, and M. Takano, *J. Solid State Chem.* **109,** 372 (1994).
12. H. Kobayashi, R. Kanno, Y. Kawamoto, T. Kamiyama, F. Izumi, and A. W. Sleight, *J. Solid State Chem.* **114,** 15 (1995).
13. R. Kanno, J. Huang, and A. W. Sleight, "Proceedings of the Fifth International Symposium on Advanced Nuclear Energy Research, Neutron as Microscopic Probes, March 1993," JAERI-M 93-228, Vol. 2, p. 347.
14. F. Izumi, "The Rietveld Method" (R. A. Young, Ed.), Chap. 13. Oxford Univ. Press, Oxford, 1993.
15. T. Kamiyama, K. Oikawa, N. Tsuchiya, M. Osawa, H. Asano, N. Watanabe, M. Furusaka, S. Satoh, I. Fujikawa, T. Ishigaki, and F. Izumi, *Physica B* **213–214,** 875 (1995).
16. W. R. Busing, K. O. Martin, and H. A. Levy, Report ORNL-TM-306. Oak Ridge National Laboratory, Oak Ridge, TN, 1964.
17. R. D. Schannon and C. T. Prewitt, *Acta Crystallogr.* **B25,** 925, (1969).
18. B. J. Kennedy and T. Vogt, *J. Solid State Chem.* **126,** 261 (1996).
19. G. R. Facer, M. M. Elcombe, and B. J. Kennedy, *Aust. J. Chem.* **46,** 1897 (1993).
20. R. A. Beyerlein, H. S. Horowitz, J. M. Longo, M. E. Leonowicz, J. D. Jorgensen, and F. J. Rotella, *J. Solid State Chem.* **51,** 253 (1984).
21. J. N. Reimers, J. E. Greedan, and M. Sato, *J. Solid State Chem.* **72,** 390 (1988).
22. J. E. Greedan, J. N. Reimers, C. V. Stager, and S. L. Penny, *Phys. Rev. B* **43,** 5682 (1991).
23. M. Sato and J. E. Greedan, *J. Solid State Chem.* **67,** 248 (1987).